J Fluoresc
DOI 10.1007/s10895-017-2115-1

ORIGINAL ARTICLE

A Colorimetric Fluorescent Probe for SO_2 Derivatives-Bisulfite and Sulfite at Nanomolar Level

Jian Zhang[1] · Aidong Peng[2] · Yanlin Lv[1] · Yuanlin Zhang[1] · Xuefei Wang[1] · Guangjin Zhang[3] · Zhiyuan Tian[1]

Received: 13 February 2017 / Accepted: 8 May 2017

Abstract A colorimetric fluorescent probe with fluorescence emission feature sensitive to SO_2 derivatives, i.e. bisulfite (HSO_3^-) and sulfite (SO_3^{2-}), was developed based on the HSO_3^-/SO_3^{2-}-mediated nucleophilic addition reaction of the probe that. This probe exhibited SO_3^{2-} sensing ability with detection limit down to 46 nM and desired selectivity over other reference anions and redox species. The preliminary fluorescence bioimaging experiments have validated the practicability of the as-prepared probe for SO_2 derivatives sensing in living cells.

Keywords Sulfur dioxide derivatives · Fluorescent probe · Bioimaging

Electronic supplementary material The online version of this article (doi:10.1007/s10895-017-2115-1) contains supplementary material, which is available to authorized users.

✉ Xuefei Wang
wangxf@ucas.ac.cn

✉ Guangjin Zhang
zhanggj@home.ipe.ac.cn

✉ Zhiyuan Tian
zytian@ucas.ac.cn

[1] School of Chemistry & Chemical Engineering, University of Chinese Academy of Sciences (UCAS), Beijing 100049, People's Republic of China

[2] College of Materials Science and Opto-Electronic Technology, University of Chinese Academy of Sciences (UCAS), Beijing 100049, People's Republic of China

[3] Key Laboratory of Green Process and Engineering, Beijing Key Laboratory of Ionic Liquids Clean Process, Institute of Process Engineering, Chinese Academy of Sciences, Beijing 100190, People's Republic of China

Introduction

Bisulfite and sulfite are substances widely involved in daily life and the general population is generally exposed to them owing to their widespread use as additives in food and beverage, cosmetic, drugs, and some fields such as leather processing, textile, and mining [1]. However, it has demonstrated that exposure to high dose of sulfite may cause adverse effects such as dermatitis, urticarial, hypotension, stomachache, diarrhea and so on [2, 3]. Specifically, sulfite may cause breathing difficulty within minutes after intake of sulfite-containing food and even low dose of sulfite would trigger bronchoconstriction of some asthma patients extremely sensitive to sulfite [4–7]. Taking these adverse effects on human health, the use of bisulfite and sulfite as additives is strictly regulated. In clinical diagnostics, high sulfite content in the blood and urine of babies has been demonstrated to be associated with molybdenum cofactor deficiency disease, which leads to neurological damage and early death unless treated [8, 9]. On the other hand sulfur dioxide (SO_2) is a kind of primary air pollutant generated from the widespread combustion of fossil fuel. The inspiratory SO_2 will hydrate and generate sulfurous acid, and then hydrolyze immediately to the corresponding bisulfite and sulfite derivatives, which mainly determine the toxicity of SO_2 [10]. Epidemiology studies indicated that the contact of SO_2 typically gives rise to a variety of respiratory tract reaction [11] and is related to lung cancer, angiocardiopathy and many kinds of neurological disorders (migraine headaches, stroke, brain tumor) [12]. Toxicology studies demonstrated that SO_2 and its derivatives are capable of changing the voltage-gated features of the sodium and potassium channels in rat hippocampus neurons [13], affecting the intracellular mercaptan content [14] and causing the neuron damage [15]. Thus, it is unequivocally crucial to develop strategies for the facile detection of bisulfite and sulfite with

Published online: 21 May 2017

high sensitivity and selectivity in biological systems. Various types of fluorescent probes selectively sensitive to SO_2 and its derivatives have been exploited [16–24]. Amoros et al. reported detection of SO_3^{2-} in aqueous milieu using organic-inorganic silica nanoparticles with limit of detection (LOD) of 0.32 ppm [16]. Based on the mechanism of Förster resonance energy transfer (FRET) between the carbon quantum dots (CDs) and merocyanine dye, Wang et al. developed fluorescent probes for HSO_3^- sensing with LOD of 1.8 μM [17]. By taking advantage of the iridium metal complexes, Chao et al. achieved the detection of SO_3^{2-} with LOD of 0.24 μM in phosphorescence mode [19].

In this work, a new type of colorimetric fluorescent probe for SO_2 derivatives sensing was developed based on 2-(2-Hydroxyphenyl) benzothiazole (HBT) conjugated with hemicyanine dye (HcD). Such type of probe, hereafter abbreviated as HBT-HcD, displayed SO_3^{2-} sensing sensitivity with detection limit down to 46 nM, obviously outperforming the counterpart probes described to date, and desired selectivity over other reference anions and redox species. It was demonstrated that the electron-deficient double bond of HBT-HcD underwent SO_3^{2-}-mediated nucleophilic addition reaction, which typically altered the π-conjugation feature of HBT-HcD and its fluorescence emission. As a typical class of fluorophore with salient excited-state intramolecular proton transfer (ESIPT) feature, HBT and its derivatives have been widely applied in the design of various fluorescent probes. Owing to the high fluorescence quantum yield of HBT [25], "turn-on" type fluorescent probe using HBT as signaling unit is anticipated to enable large contrast in analyte-triggered fluorescence response and therefore high sensitivity. On the other hand, the electron-withdrawing nature of HBT fragment [26–28] is anticipated to facilitate the SO_3^{2-}-mediated nucleophilic addition reaction that double bond undergoes by decreasing the electron density of the attacked atom, which was demonstrated to be efficient in improving the sensing sensitivity of HBT-HcD as compared to the previous counterpart probes as discussed in next section.

Results and Discussion

Synthesis of HBT-HcD Probe

HBT-HcD was synthesized following strategy as depicted in Scheme 1. In brief, the condensation reaction of 2-aminobenzenethiol with 5-methylsalicylaldehyde yielded the intermediate HBT-Me. After the protection of the hydroxyl of HBT-Me by MOMCl, the oxidation of the methyl was achieved via Sommelet reaction and HBT-CHO was therefore obtained. Following the condensation between HBT-CHO and ionized 2, 3-dimethylbenzo[d]thiazol-3-ium iodide which was derived from the reaction between 2-methylbenzothiazole and iodomethane, the target HBT-HcD probe was eventually obtained. Detailed synthetic procedures and characterization data were given in the Experimental Section.

Time-Dependent Tracking and Titration

To evaluate the response of the as-prepared HBT-HcD probe to SO_3^{2-}, fluorescence evolution features of the probe in DMSO/PBS buffer (3:7, *v*/v, 10 mM, pH 7.4) were acquired firstly. As shown in Fig. 1, the aqueous sample of HBT-HcD probe (10 μM) in the absence of SO_3^{2-} exhibited an emission band in the range of 550–650 nm with a peak around 590 nm. Upon addition of SO_3^{2-} (15 equiv), obvious changes in the fluorescence emission features of the probe was clearly observed. Specifically, the fluorescence emission intensity of the solution sample at 465 nm increased consecutively at the expense of the fluorescence emission intensity at 590 nm and reached a plateau ~30 min after the addition of SO_3^{2-}. Taking such fluorescence evolution feature, fluorescence measurement of the probe sample was performed 30 min after the addition of SO_3^{2-} in the following experiments for the fluorescence titration.

To evaluate the ability of HBT-HcD probe for SO_3^{2-} sensing, fluorescence titration was carried out with the result displayed in Fig. 2. It can be seen from Fig. 2a that the probe sample (10 μM) in DMSO/PBS buffer (3:7, *v*/v, 10 mM, pH 7.4) displayed strong absorption band centered at 517 nm. Upon increasing the concentration of SO_3^{2-} in the sample, this characteristic absorption peak gradually attenuated accompanying with a slight increment in absorption band centered at 335 nm. As a result of such change in the absorption feature, the aqueous sample of the probe clearly changed from pale pink to colorless, as illustrated in the inset in Fig. 2a, suggesting the SO_3^{2-}-mediated formation of adduct. Upon 400-nm excitation, the HBT-HcD probe in DMSO/PBS buffer displayed weak orange fluorescence emission features centered at ~590 nm, as shown in Fig. 2b. Upon incremental addition of SO_3^{2-}, a new emission band centered at ~465 nm emerged and became gradual predominance at the expense of the orange emission band. Figure 2c displayed the evolution of fluorescence intensities of the sample at 465 nm and 590 nm, respectively, as a function of the apparent concentration of SO_3^{2-} in the aqueous sample. It can be seen that upon addition of 15 equiv. of SO_3^{2-}, the blue fluorescence intensity reached a plateau accompanying with the nearly complete disappearance of the orange emission band, suggesting the SO_3^{2-}-mediated complete conversion from the probe to the adduct. Specifically, the fluorescence intensity at 465 nm of the HBT-HcD probe dramatically increased with a 150-fold enhancement factor upon the addition of 15 equiv. SO_3^{2-}. Fig. 2d displays a plot of the fluorescence intensity at 465 nm of the sample against the concentration of SO_3^{2-} and the corresponding linear fit (R^2 = 0.986) to the experimental

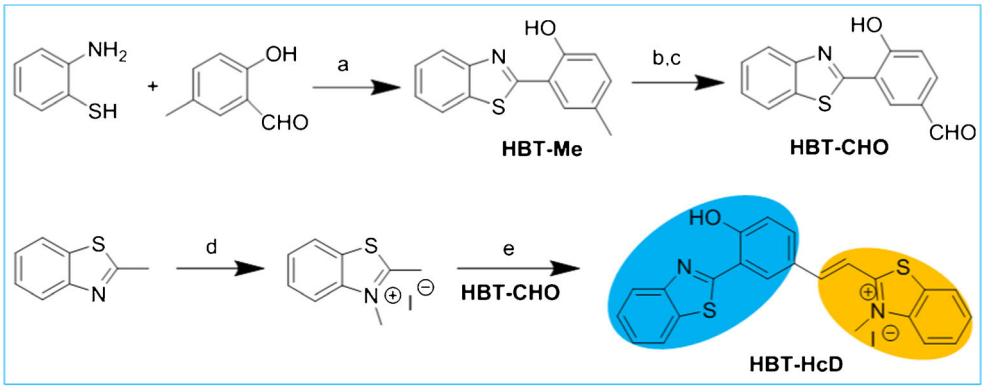

Scheme 1 Synthetic routes for the target HBT-HcD probe. *a*, H_2O_2, HCl (35%), EtOH, rt.; *b*, MOMCl, DIPEA, DCM, 0 °C, then reflux; *c*, (i) NBS, AIBN, CCl_4, reflux, (ii) HMTA, $CHCl_3$, reflux, (iii) AcOH, reflux; *d*, CH_3I, CH_3CN; e, EtOH, reflux

data. From such titration result, a detection limit of ~46 nM of HBT-HcD for SO_3^{2-} sensing was determined based on the 3-sigma method, namely, the equation of detection limit = 3σ/k, where σ is the standard deviation of blank measurement and *k* is the slope acquired from the linear fit illustrated in Fig. 2d.

The Selectivity

To evaluate the sensing selectivity of HBT-HcD probe for SO_2 derivatives, the probe was tested against various typical reference anions and redox species such as PO_4^{3-}, $H_2PO_4^-$, HPO_4^-, HSO_4^-, NO_3^-, NO_2^-, $S_2O_3^{2-}$, SO_4^{2-}, Cl^-, Br^-, I^-, F^-, CO_3^{2-}, OAc^-, HCO_3^-, PPi, ClO^-, H_2O_2, SH^-, N_2H_4, O_2^-, Cys, and GSH. Taking the aforementioned evolution feature of two characteristic emission peak as illustrated in Fig. 2b, we acquired the fluorescence intensity ratio as the measure of the fluorescence color purity of the sample in the sensing selectivity evaluation. For the fluorescence feature of free HBT-HcD probe, the fluorescence color is typically orange because the blue/orange fluorescence intensity quotient I_{465}/I_{590} = ~0.18. Upon addition of these reference anions and redox species with identical concentrations, the counterpart fluorescence intensity quotient, I_{465}/I_{590}, nearly kept unchanged or minimally affected as compared to the free HBT-HcD probe sample, as shown in Fig. 3. In sharp contrast, the addition of SO_3^{2-} with identical concentrations dramatically induced the increase of fluorescence intensity quotient I_{465}/I_{590} up to ~118, presenting a pure blue color. Thus, the fluorescence intensity quotient altered by 656 times upon addition of SO_3^{2-} to the probe sample. Similarly, the addition of SO_3^{2-} with identical concentrations led to remarkable fluorescence change from orange to blue with significant fluorescence intensity quotient alteration. These results suggest a high selectivity of the as-prepared probes for SO_2 derivatives over other anions and indicate the diagnostic potential of the probe for HSO_3^-/SO_3^{2-} sensing in biological samples. Inset in Fig. 3b illustrates the photographs of HBT-HcD probe (10 μM) with various anions and redox species under the illumination of a hand-held UV lamp with λ_{ex} = 365 nm. Obviously, only the probe sample in the presence of HSO_3^-/SO_3^{2-} displayed vivid cyan fluorescence while the sample in the presence of reference anions and redox species exhibit orange-red as the same color to the free aqueous HBT-HcD probe sample, indicating the reliable selectivity of the probe for HSO_3^-/SO_3^{2-} sensing.

To evaluate the recognition specificity of HBT-HcD probe to SO_2 derivatives, competitive reaction experiments of the probe with sulfite in the presence of interference anions and redox species were performed. Typically, fluorescence

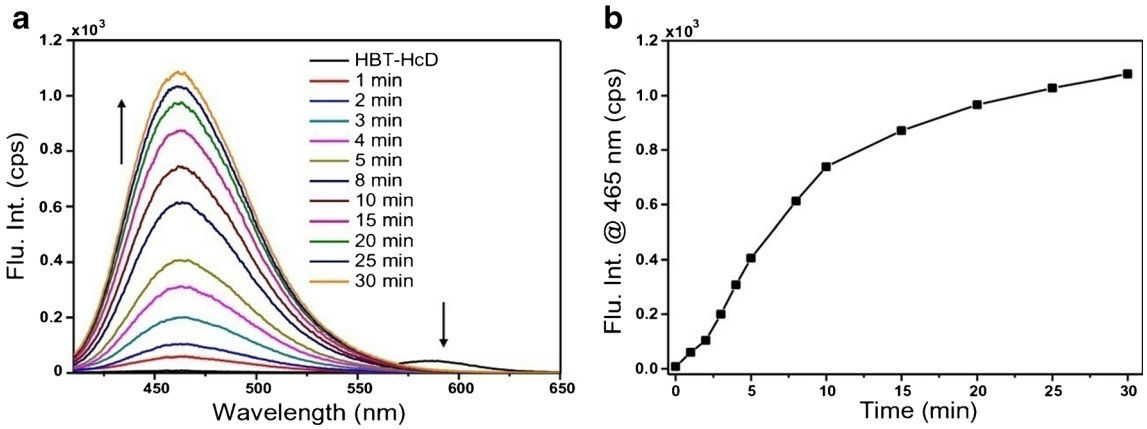

Fig. 1 Time-elapsed fluorescence emission spectra of the aqueous HBT-HcD probe (10 μM) in DMSO/PBS buffer (3:7, *v*/v, 10 mM, pH 7.4, 37 °C) sample upon addition of SO_3^{2-} (15 equiv)

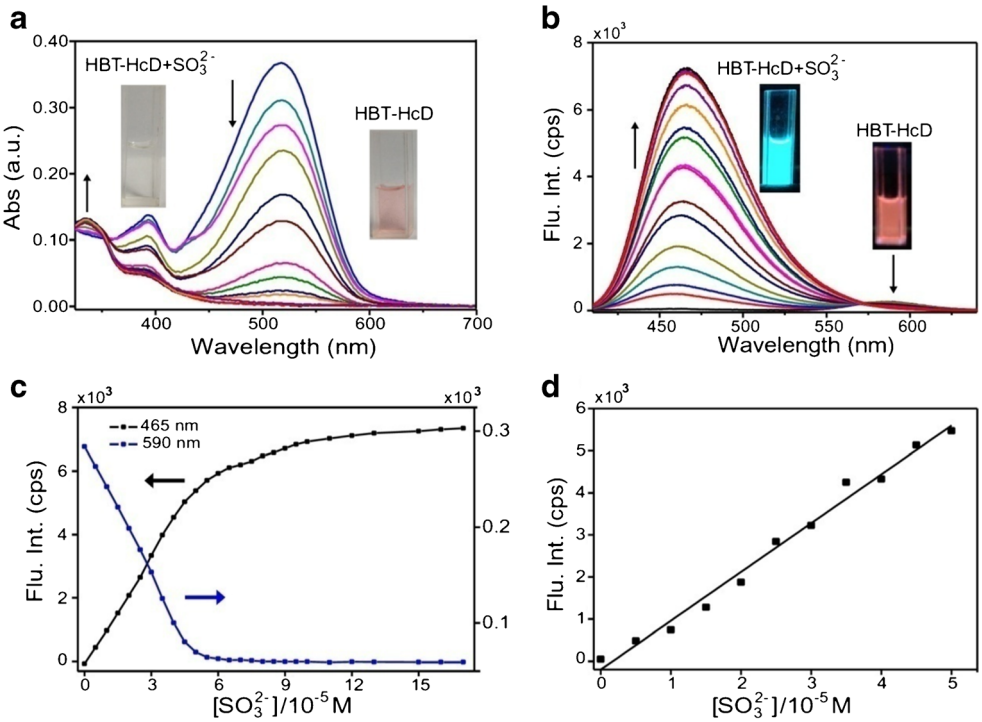

Fig. 2 (**a**) Absorption and (**b**), (**c**) fluorescence titration profile of HBT-HcD probe (10 μM) in DMSO/PBS buffer (3:7, *v*/v, 10 mM, pH 7.4, 37 °C) with SO_3^{2-} with different concentrations and (**d**) the corresponding plot of fluorescence intensity (at 465 nm) of the aqueous HBT-HcD probe as a function of SO_3^{2-} concentration. λ_{ex} = 400 nm

intensity quotient (I_{465}/I_{590}) of the probe in DMSO/PBS buffer in the presence of 10 equiv. of SO_3^{2-} and various interference anions, respectively, were acquired firstly and then the counterpart fluorescence intensity ratio of the abovementioned samples with subsequent addition of 10 equiv. of SO_3^{2-} were acquired under the identical condition. By comparing the change in the fluorescence intensity ratio of each pair of probe samples, namely, samples before and after the addition of SO_3^{2-}, the response performances of the probe to SO_3^{2-} at the presence of various interference anions were obtained. As illustrated in Fig. S1(ESI), these reference anions could hardly interfere with the HSO_3^-/SO_3^{2-}-induced fluorescence evolution of HBT-HcD probe, definitely indicating the recognition specificity of the probe to SO_2 derivatives.

The Effect of pH on HBT-HcD

The effect of pH on the fluorescence emission features of the HBT-HcD probe was also investigated. Figure 4 displayed the fluorescence intensity quotient of HBT-HcD probe in DMSO/PBS buffer (3:7, *v*/v, 10 mM) with various pH values in the absence and presence of SO_3^{2-}. It can be clearly seen that the fluorescence intensity quotient (I_{465}/I_{590}) of the free probe sample did not displayed discernable change upon changing the pH value in the range of pH 4.0–10.0, suggesting the good stability of the probe even in such broad range of acidic/alkaline milieu. Furthermore the HBT-HcD probe sample in the presence of SO_3^{2-} exhibited excellent response feature in the range of pH 6.0–8.0, indicating its potential in biological applications.

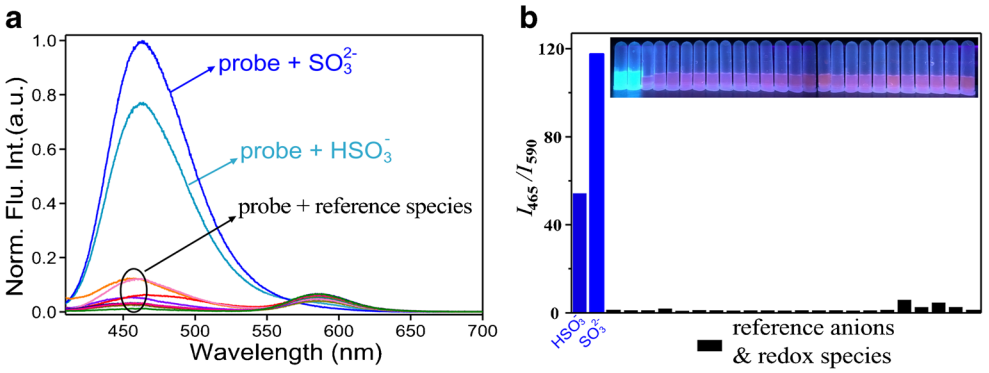

Fig. 3 (**a**) Fluorescence emission spectra of HBT-HcD probe (10 μM) in DMSO/PBS buffer (3:7, *v*/v, 10 mM, pH 7.4, 37 °C) in the absence and presence of HSO_3^-/SO_3^{2-}, reference anions (10 equiv). (**b**) Fluorescence intensity ratio (I_{465}/I_{590}) response of the probe to HSO_3^-/SO_3^{2-}, reference and anions. Inset: photographs of HBT-HcD probe (10 μM) in the absence and presence of HSO_3^-/SO_3^{2-}, reference anions under the illumination of a hand-held UV lamp with λ_{ex} = 365 nm

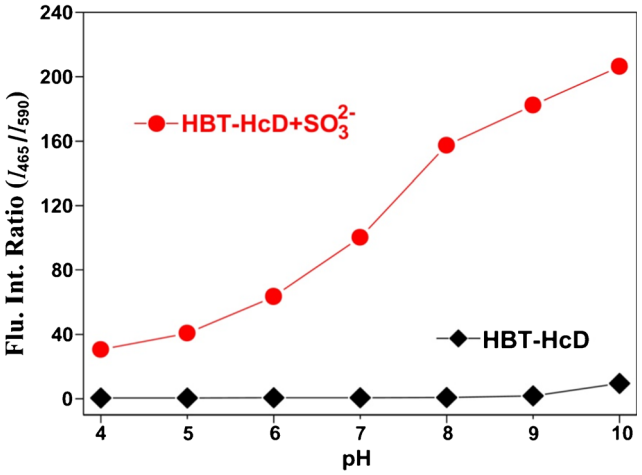

Fig. 4 The pH-dependent fluorescence intensity quotient (I_{465}/I_{590}) of the probe in DMSO/PBS buffer (3:7, *v*/v, 10 mM) in the absence and presence of SO_3^{2-}

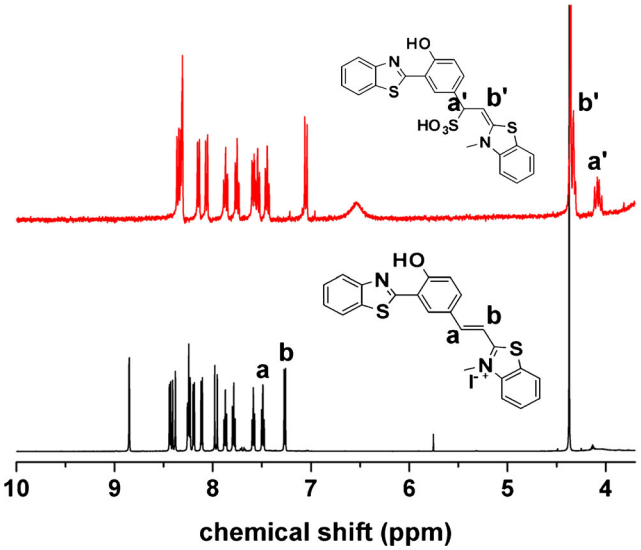

Fig. 5 The proposed response mechanism of HBT-HcD to SO_3^{2-} and partial ^{1}H NMR spectra of HBT-HcD in deuterated DMSO/D_2O upon addition of SO_3^{2-} (10 equiv)

The Sensing Mechanism

For molecular structure of HBT-HcD probe, HBT moiety is integrated into the molecular skeleton of HcD and is a part of the delocalized electron system. Electron communication between these two moieties enables extended π-conjugation that typically generates low energy fluorescence emission. Upon addition reaction with nucleophilic agent SO_3^{2-}, the π-conjugate bridge (double bond) is broken and the delocalization of π-electron is therefore interrupted. For the adduct product, HBT moiety is not part of the delocalized electron system and the excitation is localized on the HBT moiety. As a result, fluorescence emission originating from the locally excited state of HBT moiety is restored, shifting the fluorescence emission from orange (centered at ~590 nm) to cyan (centered at ~465 nm). To verify such proposed sensing mechanism of HBT-HcD probe for SO_3^{2-}, ^{1}H NMR titration was carried out in mixed deuterated DMSO and D_2O with the results shown in Fig. 5. It is conjectured that the hydrolysis of SO_3^{2-} to HSO_3^- occurred before the nucleophilic attack to HBT-HcD. Specifically, the signals at 7.26–7.27 and 7.48–7.50 ppm (denoted a and b) in the ^{1}H NMR spectrum attributable to the double bond in HBT-HcD vanished and simultaneously the signals at 4.07/4.33 ppm that can be assigned to the methyne (denoted a' and b') of the addition product respectively, clearly appeared. Additionally, other signals belong to the aromatic ring were found up-shifted to the high field. In addition to the information from the ^{1}H NMR titration, the proposed mechanism of HBT-HcD probe for SO_3^{2-} sensing also found support from the ESI-MS characterization results of the HBT-HcD probe sample in the absence and presence of SO_3^{2-}. Specifically, the adduct product of the probe upon addition of SO_3^{2-} displayed characteristic mass-to-charge ratios at m/z = 505.2 [M + Na^+], which is in well agreement with the calculated m/z values of the structures of HBT-HcD + HSO_3^-. Definitely, the ^{1}H NMR and ESI-Mass characterization results validated the abovementioned proposed sensing mechanism of the as-prepared HBT-HcD probe. Based on the similar mechanism, namely SO_3^{2-}-mediated addition reaction, Yang et al. developed another type of fluorescent probe for sulfite sensing characterized with sulfite-induced fluorescence decrease and detection limit of 0.1 μM [29].

Taking the nature of analyte-mediated nucleophilic addition reaction that HBT-HcD and other fluorescent probes with similar structural features undergo, decreasing the electron density of the active sites in the molecular skeleton of the probes is anticipated to facilitate the nucleophilic attack and therefore improve the sensing sensitivity. To verify such speculation, the natural bonding orbital (NBO) charge distribution of HBT-HcD was acquired via geometry optimization at the level of B3LYP/6-31G (d) and the counterpart feature of another model molecule with molecular structure closely related to that of HBT-HcD, abbreviated as coumarin-HcD, was investigated for comparison. It is noted that the replacement of HBT moiety by coumarin constitutes the whole difference between the molecular structure of HBT-HcD and that of coumarin-HcD, as illustrated in Fig. 6. It also deserves mentioning that the coumarin groups without specific functionalization typically do not display appreciable electron-withdrawing characteristics [30] and they may function as electron-donating moieties in some cases [31]. It can be clearly seen from the optimization results that the net atomic charge of the target double bond carbon atom residing in HBT-HcD skeleton is approximately 0.1 less than the counterpart charge in coumarin-HcD (−0.075 vs. -0.173). Such significant difference in net atomic charge of the active carbon atoms is expected to lead to great discrepancy in reactivity of the probes with nucleophilic agents. Specifically, the much

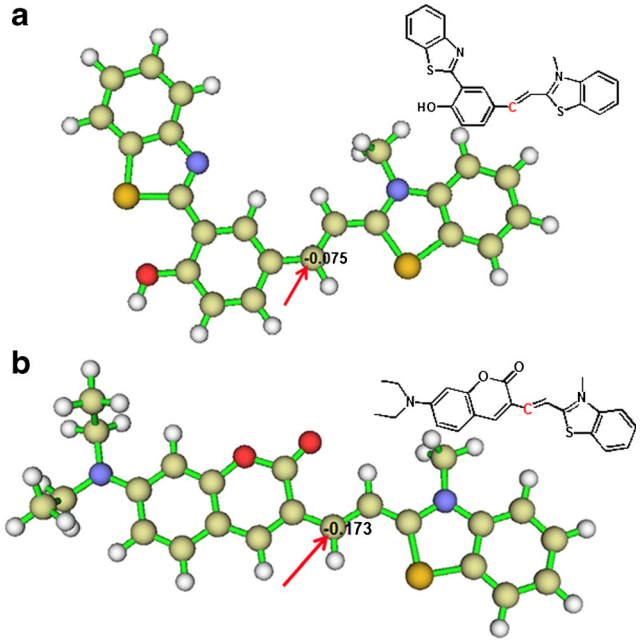

Fig. 6 Net Atomic Charges of HBT-HcD (**a**) and coumarin-HcD (**b**). The *arrows* indicate the attacked carbon atoms. Optimization of the structures were performed using B3LYP/6-31G* with Gaussian 03

lower electron density of the active carbon atom in HBT-HcD owing to the more prominent electron-withdrawing characteristics of HBT fragment is anticipated to impart higher reaction activity of HBT-HcD in nucleophile-mediated addition reaction [28]. Such improved reaction activity, together with the high fluorescence quantum yield of HBT, contributes to the excellent sensitivity of HBT-HcD to SO_3^{2-}/HSO_3^-.

Bioimaging

The applicability of the HBT-HcD probe for intracellular SO_3^{2-} sensing was also confirmed. Prior to the fluorescence cell imaging experiment, the cytotoxicity of the probe in the milieu of DMSO/PBS buffer we evaluated. Specifically, MTT assay was used to evaluate the viability of MCF-7 cells treated with various concentrations of HBT-HcD ranging from 0 to 10 μM. As illustrated in Fig. S2 (ESI), although the cell viability displayed gradual decrease upon increasing the feeding amount of HBT-HcD probe stock solution in DMSO/PBS buffer, nearly 84% cells survived in the case of cells incubation with the HBT-HcD probe with the concentration up to10 μM for 24 h. Thus, the HBT-HcD probe in the milieu of DMSO/PBS buffer possesses good biocompatibility for cell imaging. In a typical intracellular SO_3^{2-} sensing experiment, MCF-7 cells were incubated with 10 μM HBT-HcD probe in Dulbecco's Modified Eagle's Medium (DMEM medium) at 37 °C for 30 min before the acquisition of the differential interference contrast (DIC) (Fig. 7a) and fluorescence images of the cells via confocal laser scanning microscopy (CLSM). It can be seen that the cells with internalized HBT-HcD probes exhibit discernible fluorescence in red channel (Fig. 7c), but not in blue channel (Fig. 7b). Subsequently, the cells were treated with SO_3^{2-} for another 30 min at 37 °C and then the fluorescence images of the cells in both channels were acquired. In sharp contrast to the favorable fluorescence of the cells in red channel before the addition of SO_3^{2-}, the fluorescence the cells acquired after

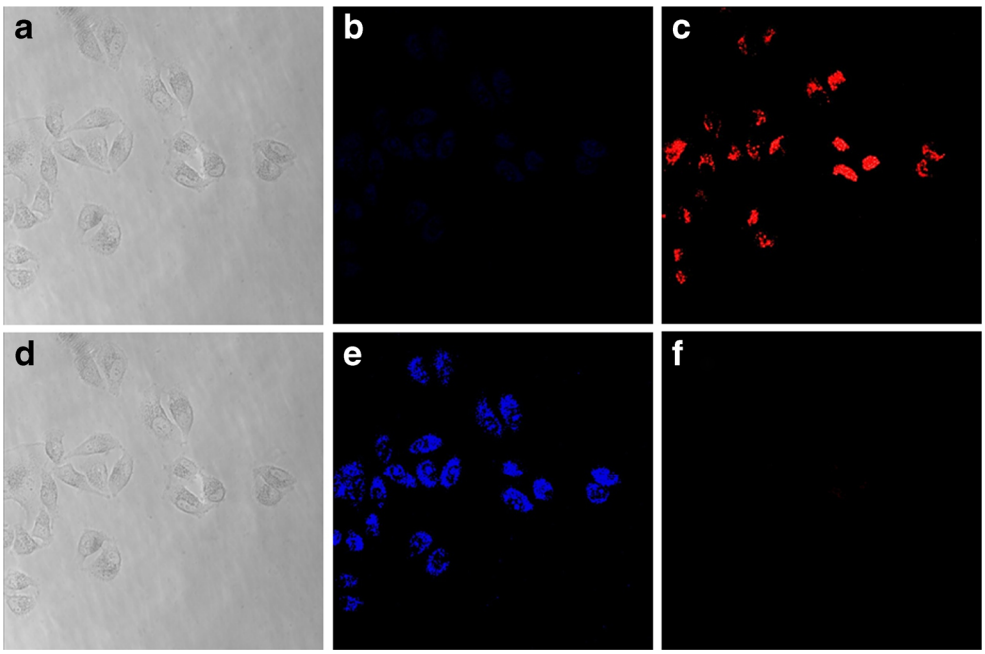

Fig. 7 Differential interference contrast (DIC) and confocal laser scanning microscopy (CLSM) fluorescence images of HBT-HcD probe in intracellular SO_3^{2-} sensing. (**a**) The DIC image of MCF-7 cells after incubation with HBT-HcD probe; (**b**) and (**c**) the CLSM fluorescence images of MCF-7 cells after incubation with HBT-HcD probe acquired via blue- and orange-channel, respectively. (**d**) The DIC image of cells shown in (**a**, **b** and **c**) upon further incubation with SO_3^{2-}; (**e** and **f**) the CLSM fluorescence images of cells shown in (**d**) upon further incubation with SO_3^{2-} acquired via blue- and orange-channel, respectively

the addition of SO_3^{2-} in red channel was vanished (Fig. 7f), meanwhile exhibited cellular contours with much stronger brightness in blue channel (Fig. 7e). Unequivocally, such a dramatic contrast in two fluorescence channels clearly demonstrated the usefulness of the as-prepared HBT-HcD probe for intracellular SO_3^{2-} sensing.

Conclusion

In conclusion, a new type of colorimetric fluorescent probe HBT-HcD for SO_2 derivatives (SO_3^{2-}/HSO_3^-) sensing with high selectivity over other reference anions and redox species was developed in the present work. Upon the SO_3^{2-}/HSO_3^--mediated nucleophilic addition reaction of the double bond in HBT-HcD molecular skeleton, the aqueous sample of the probe clearly changed from pale pink to colorless; on the other hand the fluorescence emission peak at 465 nm attributable to the locally excited state of HBT moiety lighted up at the expense of the emission band centered at 590 nm originating from HBT-HcD with extended π-conjugation system. The geometry optimization result indicated that the HBT fragment characterized with electron-withdrawing feature contributed to the decreased electron density of the active carbon atoms in the HBT-HcD molecular skeleton, which was anticipated to facilitate the nucleophilic attack in the SO_3^{2-}/HSO_3^--mediated nucleophilic addition reaction. Owing to the salient electron characteristics and high fluorescence quantum yield of HBT moiety, improved sensing sensitivity of the probe to SO_3^{2-} with limit of detection down to 46 nM was achieved. The preliminary dual-channel fluorescence bioimaging experiments have validated the practicability of the as-prepared HBT-HcD for SO_2 derivatives sensing in living cells.

Experimental Section

General

All chemicals were purchased from J&K Chemicals or Energy and used as received. PL spectra were recorded on a spectrofluorophotometer (F-7000, Japan). UV absorption spectra were taken on U-4100 UV-Vis spectrophotometers. Both UV-vis spectra and fluorescent spectra were acquired with 10 mm-light path standard quartz cuvettes. ^{1}H and ^{13}C NMR spectra were measured on a Bruker Avance 600 MHz NMR spectrometer in deuterated $CDCl_3$ and deuterated DMSO with tetramethylsilane (TMS; δ = 0 ppm) as internal standard. Electrospray mass spectra (ESI-MS) were recorded on Agilent 1100 Series.

Synthesis of Probe HBT-HcD

2-(benzo[d]thiazol-2-yl)-4-methylphenol (HBT-Me)

To the solution of 2-aminobenzenethiol (832 mg, 6.6 mmol) and 5-methylsalicylaldehyde (900 mg, 6.6 mmol) in absolute ethanol (30 mL) was added H_2O_2 (0.915 mL, 30 mmol) and concentrated hydrochloric acid (0.465 mL,15 mmol) at room temperature. After 3 h the mixture was filtered off and washed with ethanol for three times and then dried in vacuum to afford HBT-Me for 1.2 g (yield, 75%).^{1}H NMR (600 MHz, $CDCl_3$): δ 12.30(1H, s), 7.97–7.98 (1H, d, J = 8.4 Hz), 7.89–7.90 (1H, d, J = 7.8 Hz), 7.47–7.50 (2H, m), 7.40–7.41 (1H, m), 7.18–7.19 (1H, m), 7.00–7.02 (1H, d, J = 8.4 Hz), 2.36 (3H, s); ^{13}C NMR (150 MHz, $CDCl_3$): δ 163.38, 154.78, 150.90, 132.70, 131.58, 127.64, 127.29, 125.59, 124.39, 121.09, 120.45, 116.63, 115.31, 19.44. MS (ESI) m/z 240.1(M-1).

2-(2-(methoxymethoxy)-5-methylphenyl)benzo[d]thiazole (HBT-MOM)

To the solution of HBT-Me (747 mg, 3.1 mmol) and DIPEA (4.1 mL, 23.25 mmol) in dried dichloromethane was added MOMCl (1.8 mL, 23.25 mmol) dropwise at 0 °C. Then the mixture was refluxed for 10 h, after the solution was extracted with saturated sodium bicarbonate. The organicphase was concentrated in vacuum and then the residue was purified by column chromatography on silica gel (dichloromethane: petroleum ether = 2:1) to afforded HBT-MOM for 857 mg (yield, 97%). ^{1}H NMR (600 MHz, $CDCl_3$): δ 8.34–8.35(1H, m), 8.10–8.11(1H, d, J = 8.1 Hz), 7.92–7.93 (1H, d, J = 7.6 Hz), 7.48–7.49 (1H, m),7.38–7.39 (1H, m),7.22–7.26 (1H, m), 7.17–7.18 (1H, d, J = 8.4 Hz), 5.39 (2H, s), 3.56 (3H, s), 2.41 (3H, s); ^{13}C NMR (150 MHz, $CDCl_3$): δ 163.22, 152.79, 152.12, 136.08, 132.36, 131.66, 129.57, 125.91, 124.61, 122.77, 122.51, 121.14, 114.75, 94.53, 56.56, 20.50. MS (ESI) m/z 286.1 (M + 1).

3-(benzo[d]thiazol-2-yl)-4-hydroxybenzaldehyde (HBT-CHO)

To a solution of HBT-MOM (612 mg, 2.15 mmol) in tetrachloromethane (50 mL) was added NBS (463 mg, 2.6 mmol) and AIBN (107 mg, 0.65 mmol). The resulting solution was refluxed for 24 h, after which the tetrachloromethane was distilled to afford yellow residue, which was extracted with dichloromethane of 100 mL and saturated sodium thiosulfate. The organic phase was concentrated in vacuum and then the residue was added to the solution of hexamethylenetetramine (HMTA) (900 mg, 6.5 mmol) in chloroform (30 mL). The resulting solution was refluxed for 18 h, after which the chloroform was distilled to afford white residue, to which 20 mL acetic acid was added. The mixture was refluxed for 2 h and

then cooled to room temperature and 100 mL ethyl acetate was added. The solution was neutralized with saturated sodium carbonate and then washed with saturated brine. The organic phase was concentrated in vacuum and the residue was purified by column chromatography on silica gel (dichloromethane: petroleum ether = 1:1) to afforded HBT-CHO for 97 mg (yield, 18%).^{1}H NMR (600 MHz, $CDCl_3$): δ 13.36 (1H, s), 9.95 (1H, s), 8.25–8.26(1H, d, J = 1.8 Hz), 8.03–8.04 (1H, d, J = 7.8 Hz),7.96–7.97 (1H, d, J = 7.8 Hz),7.91–7.93 (1H, dd, J = 1.8 Hz, J = 8.4 Hz), 7.54–7.57 (1H, m), 7.46–7.49 (1H, m), 7.22–7.23 (1H, d, J = 8.4 Hz); ^{13}C NMR (150 MHz, $CDCl_3$): δ 189.89, 168.24, 163.09, 151.34, 133.91, 132.58, 130.68, 128.84, 127.05, 126.15, 122.35, 121.72, 118.71, 117.10. MS (ESI) m/z 254.1 (M-1).

2,3-dimethylbenzo[d]thiazol-3-ium Iodide

To 30 mL of CH_3CN was added 2-methylbenzothiazole (2.98 g, 20 mmol) and methyl iodide (2.8 g, 20 mmol), the mixture was refluxed under Ar for 24 h and then cooled to ambient temperature, the white solid was filtered off and washed with CH_3CN for three times and then dried in vacuum to afford 2,3-dimethylbenzo[d]thiazol-3-ium iodide for 5.1 g (yield, 88%).^{1}H NMR (600 MHz, d^6-DMSO): δ 8.46–8.47 (1H, d, J = 8.4 Hz), 8.29–8.30 (1H, d, J = 8.4 Hz), 7.87–7.89 (1H, m), 7.78–7.80 (1H, m), 4.22 (3H, s), 3.20 (3H, s); ^{13}C NMR (150 MHz, d^6-DMSO): δ 177.10, 141.54, 129.21, 128.65, 128.00, 124.51, 116.76, 36.45, 17.46. MS (ESI) m/z 164.0 (M-I¯).

2-(3-(benzo[d]thiazol-2-yl)-4-hydroxystyryl) -3-methylbenzo[d]thiazol-3-iumiodide (HBT-HcD)

To 50 mL of absolute ethanol was added 2,3-dimethylbenzo[d]thiazol-3-ium iodide (145 mg, 0.5 mmol) and HBT-CHO (130 mg, 0.5 mmol), the mixture was refluxed under Ar for 36 h and then cooled to ambient temperature, the mixture was concentrated in vacuum and the residue was purified by column chromatography on silica gel (dichloromethane: methanol = 10:1) to afforded HBT-HcD for 170 mg (yield, 64%).^{1}H NMR (600 MHz, d^6-DMSO): δ 12.53 (1H, br), 8.85–8.86 (1H, d, J = 1.8 Hz), 8.39–8.45(2H, m), 8.23–8.26 (2H, m), 8.19–8.21 (1H, d, J = 7.8 Hz),8.11–8.12 (1H, d, J = 7.8 Hz),7.96–7.98 (1H, d, J = 15.6 Hz), 7.86–7.89 (1H, t, J = 7.8 Hz), 7.78–7.80 (1H, t, J = 7.8 Hz), 7.58–7.60 (1H, t, J = 7.8 Hz), 7.48–7.51 (1H, t, J = 7.8 Hz), 7.26–7.28 (1H, d, J = 8.4 Hz), 4.38 (3H, s); ^{13}C NMR (150 MHz, d^6-DMSO): δ 172.08, 163.33, 159.82, 151.32, 148.40, 142.00, 134.80, 132.65, 132.07, 129.27, 128.23, 127.72, 126.58, 126.09, 125.28, 124.18, 122.24, 122.12, 119.53, 118.00, 116.69, 111.80, 48.56. MS (ESI) m/z 401.2 (M-I¯).

General Procedure for Cell Imaging

MCF-7 cells were cultured in media (GIBCO RPMI 1640 supplemented with 10% FBS, 100 units per mL of penicillin and 100 units per mL of streptomycin) at 37 °C in a humidified incubator, and culture media were replaced with fresh media every day. The cells were further incubated with 10 μM of probe in culture media for 15 min at 37 °C and then washed 3 times with warm PBS buffer before cell fluorescence imaging experiments with confocal laser scanning microscopy.

Acknowledgements Financial support from the National Natural Science Foundation of China (grant no. 21373218 and 21573234) is acknowledged.

References

1. Council Directive (1995) 95/2/EC of the European Parliament and of the Council of 20 February 1995 on food additives other than colors and sweeteners. Official J Eur Communities 18.3., L 61, 1
2. Vally H, Misso NLA, Madan V (2009) Clin Exp Allergy 39:1643
3. Niknahad H, O'Brien PJ (2008) Chem Biol Interact 174:147
4. Oliphant T, Mitra A, Wilkinson M (2012) Contact Dermatitis 66:128
5. Garcia-Ortega P, Scorza E, Teniente A (2010) Clin Exp Allergy 40:688
6. Vally H, Thompson PJ, Misso NLA (2007) Clin Exp Allergy 37:1062
7. Bush RK, Taylor SL, Holden KJ, Nordlee A, Busse WW (1986) Am J Med 81:816
8. Joint FAO/WHO,JECFA,(2009) WHO FOOD ADDITIVES SERIES:60
9. U.S. Environmental Protection Agency(2003) Toxicological Review of Hydrogen sulfide
10. Meng ZQ, Qin GH, Zhang B, Bai JL (2004) Mutagenesis 19:465
11. Iwasawa S, Kikuchi Y, Nishiwaki Y, Nakano M, Michikawa T, Tsuboi T (2009) J Occup Health 51:38
12. Sang N, Yun Y, Li H, Hou L, Han M, Li GK (2010) Toxicol Sci 114:226
13. Li GK, Sang N (2009) Ecotoxicol Environ Saf 72:236
14. Migliore L, Coppede F (2009) Mutat Res 674:73
15. Sang N, Yun Y, Yao G, Li H, Guo L, Li G (2011) Toxicol Sci 124:400
16. Santos-Figueroa LE, Gimenez C, Agostini A, Aznar E, Marcos MD, Sancenon F, Martinez-Manez R, Amoros P (2013) Angew Chem Int Ed 52:13712
17. Sun M, Yu H, Zhang K, Zhang Y, Yan Y, Huang D, Wang S (2014) Anal Chem 86:9381
18. Chen W, Fang Q, Yang D, Zhang H, Song X, Foley J (2015) Anal Chem 87:609
19. Li GY, Chen Y, Wang JQ, Lin Q, Zhao J, Ji LN, Chao H (2013) Chem Sci 4:4426
20. Zhu L, Xu J, Sun Z, Fu B, Qin C, Zeng L, Hu X (2015) Chem Commun 51:1154
21. Wu MY, Li K, Li CY, Hou JT, Yu XQ (2014) Chem Commun 50:183
22. Sun YQ, Liu J, Zhang J, Yang T, Guo W (2013) Chem Commun 49:2637
23. Chen S, Hou P, Wang J, Song X (2012) RSC Adv 2:10869

24. Zhou HJ, Zhao YS, Gao G, Li SQ, Lan JB, You JS (2013) J Am Chem Soc 135:14908
25. Cheng JL, Liu D, Bao LJ, Xu K, Yang Y, Han KL (2014) Chem Asian J 9:3215
26. Gautam P, Misra R, Siddiqui SA, Sharma GD (2015) Org Electron 19:76
27. Bouzayen N, Zaidi B, Mabrouk A, Chemek M, Alimi K (2012) Comput Theor Chem 984:1
28. Hrobárik P, Hrobáriková V, Sigmundová I, Zahradník P, Fakis M, Polyzos I, Persephonis P (2011) J Org Chem 76:8726
29. Yang XF, Cui Y, Li YX, Zheng LY, Xie LJ, Ning R, Liu Z, Lu JL, Zhang GG, Liu CX, Zhang GY (2015) Spectrochim Acta A Mol Biomol Spectrosc 137:1055
30. Dai X, Wang ZY, Du ZF, Cui J, Miao JY, Zhao BX (2015) Anal Chim Acta 900:103
31. Chen WQ, Fang Q, Yang DL, Zhang HY, Song XZ, Foley J (2015) Anal Chem 87:609